A Numerical Simulation of a Two-phase Flow

Li Chen and Yuguo Li
Advanced Thermo-fluids Technologies Laboratory
CSIRO Building, Construction and Engineering
Highett, Victoria 3190, Australia

Abstract Modelling of multiphase flow has attracted much attention in recent years, because of its extensive industrial and environmental applications. One of the challenges in modelling multiphase fluid systems is to accurately capture the discontinuously interfacial phenomena. For example, the process of mixing can generate large changes in interfacial areas through the action of vorticity via stretching, tearing and folding. The volume tracking techniques remain quite effective for capturing fluid interfaces if some improvements to the original VOF method are considered. The improved volume tracking method allows interfaces to be captured and maintained compactly in one cell without imposing restrictions on the topological complexity or the number of interfaces that can be represented. In this paper, a modified VOF, which combines with a semi-implicit algorithm (SIMPLE) coupled with a higher-order advection scheme, is presented. The surface tension force is modelled by a continuum surface force approximation. An efficient solver is used for the resulting system of the linear equations. An example problem simulated in this paper is the buoyancy-driven motion of multi-bubbles in a viscous liquid. The complex topological change which occurred during bubbles rising is well predicted. The results are verified by the experimental data in the literature.

1. INTRODUCTION

Flows with spatial variation of fluid properties, such as gas-liquid interface due to density variation, can be found in many engineering applications. The generation of vorticity by the interaction of non-parallel pressure and discontinuous fluid properties produces a complex flow structure and scale, which presents a computational challenge. A robust algorithm for solving multi-phase flows with an accurate representation of interfaces is required to accommodate the complex topological changes of this type of flow.

Conventional algorithms for the solution of flows with an interface are associated with an explicit scheme for momentum advection on a staggered grid (e.g. Lafaurie et al. [1994], and Unverdi and Tryggvason [1992]). The use of an explicit scheme reduces the computational efficiency due to limitations in the maximum time step. At the same time, staggered grids present some difficulties for three-dimensional flows with complex geometries. Recently, a second-order time-accurate algorithm based on the Godunov technique has been developed to simulate such a flow by Rider et al. [1995]. In their projection algorithms, the convection terms are explicitly discretised with a second-order upwind scheme in a flux-limited fashion.

The boundary integral [Ryskin and Leal 1984] and Lagrangian finite element [Unverdi and Tryggvason 1992] methods are able to simulate flows with interfaces, but it is difficult for them to handle the fragmentation and coalescence of complex interfacial phenomena. The Marker and Cell (MAC) and volume tracking techniques (VOF) due to Hirt and Nichols [1982] remain quite effective. In the conventional MAC methods, the interface is represented by Lagrangian marker particles advected by the local velocity. As a result, it can not accurately define an interface, especially for three-dimensional flow, and properly conserve mass. One favoured feature of this method is that no numerical diffusion exists as any other conventional interface tracking algorithms have. Therefore, some variations of this method can still be promising [Rider et al. 1995].

In this paper, a method is presented to simulate multi-phase flows with complex interfacial phenomena on collocated grids. The method is conservative for both mass and momentum. A semi-implicit scheme is used. The velocity-pressure coupling is based on SIMPLE.

2. PROBLEM FORMULATION

Consider two spherical gas bubbles, referred to as leading and following bubbles, rising through a viscous liquid (see Figure 1).

The two bubbles are initially stationary and the coalescence of the two bubbles may occur while they are rising due to buoyancy force. In this study, both gas and liquid are considered to be incompressible and Newtonian. The motion of the bubbles is governed by the Navier-Stokes equation, which can be written in a non-dimensional form as

$$\nabla \cdot \mathbf{U} = 0$$

$$\frac{\partial(\rho\mathbf{U})}{\partial t}+\nabla\bullet(\rho\mathbf{U}\otimes\mathbf{U})=-\nabla p+\rho\mathbf{g}+\frac{1}{\mathrm{Re}}\nabla\bullet\left[\mu\left(\nabla\mathbf{U}+\nabla\mathbf{U}^{\mathrm{T}}\right)\right]+\frac{1}{Bo}\mathbf{F}_{sv} \quad (2)$$

with scales

$$p^{*}=\frac{p}{p_{ref}},\ \mathbf{U}^{*}=\frac{\mathbf{U}}{u_{ref}},\ \mathbf{x}^{*}=\frac{\mathbf{x}}{R_0},\ \tau=\frac{t}{t_{ref}}$$
$$\rho^{*}=\frac{\rho}{\rho_{ref}},\quad \mu^{*}=\frac{\mu}{\mu_{ref}},\quad \sigma^{*}=\frac{\sigma}{\sigma_{ref}} \quad (3)$$

in which

$$u_{ref}=\sqrt{gR_0},\quad p_{ref}=\rho_r u_{ref}^2 \quad (4)$$

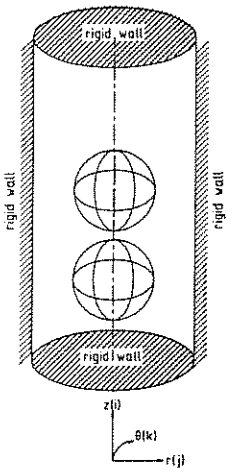

Figure 1: Schematic description of problem

Note that * is omitted in equations (1) and (2) for convenience. ⊗ denotes the inner product of tensors, $\mathbf{U}(u_r,u_\theta,u_z)$ is the fluid velocity in $\mathbf{x}(r,\theta,z)$, ρ the density, μ the dynamic viscosity, p the pressure, $\mathbf{g}(0,0,g)$ the gravity vector, R_0 initial bubble radius, and $\mathbf{F}_{sv}$ the volume form of the surface tension force. Reynolds and Bond numbers are defined as

$$\mathrm{Re}=\frac{\rho_f g^{1/2}R_0^{3/2}}{\mu_{ref}},\quad Bo=\frac{\rho_f gR_0^2}{\sigma}$$

respectively, and

$$\rho(\mathbf{x},t)=F(\mathbf{x},t)\rho_f+[1-F(\mathbf{x},t)]\rho_g \quad (5)$$
$$\mu(\mathbf{x},t)=F(\mathbf{x},t)\mu_f+[1-F(\mathbf{x},t)]\mu_g \quad (6)$$

where F is the local volume fraction of liquid. Its value is unity in the liquid phase and zero in the gas phase. The last term of equation (2) is the surface tension force which exists only at the interface. The surface tension force is modelled by the continuum surface tension force (CSF) method developed by Brackbill et al. [1992]. In this model, an interface is interpolated as a transient region with a finite thickness. Thus the surface tension force localised in this region can be converted into a volume force with the help of a Dirac delta function concentrated on the surface. The surface tension force is written as

$$\mathbf{F}_{sv}=\sigma\kappa(\mathbf{x})\frac{\nabla\tilde{c}(\mathbf{x})}{[\tilde{c}]} \quad (7)$$

in which

$$\kappa=-(\nabla\cdot\hat{\mathbf{n}}) \quad (8)$$

From the definition of a unit normal to a surface

$$\hat{\mathbf{n}}=\frac{\nabla\tilde{c}}{|\nabla\tilde{c}|} \quad (9)$$

$\tilde{c}$ in the above equations is a colour function $[\tilde{c}]$ is the difference of the colour function between two phase. Equation (8) can be expanded in terms of the unit normal to a surface, **n**, as

$$\kappa=\frac{1}{|\mathbf{n}|}\left[\left(\frac{\mathbf{n}}{|\mathbf{n}|}\cdot\nabla\right)|\mathbf{n}|-(\nabla\cdot\mathbf{n})\right] \quad (10)$$

This formulation seems to produce a better calculation of surface tension because it uses a wider stencil than equation (8).

It is noted that equations (5) and (6) represent discontinuous properties of fluid, which imply an interface between multiphase fluids, and they can be used to monitor the dynamics of the interface. However, when a large discontinuity is involved, for example a discontinuity of 850 in density ratio exists for a water-air system, numerical difficulties may arise in identifying an 'exact' interface. Thus, instead of solving equation (1) directly, the volume fraction of liquid, F, is used to identify an interface. The transport of this function is given by

$$\frac{\partial F}{\partial t}+\nabla\cdot(\mathbf{U}F)=0 \quad (11)$$

Also, the colour function in equations (7) and (9) can be replaced by the function F. We now require suitable initial and boundary conditions. In the case studied in this paper, an initially spherical gas bubble is located on the axis of a vertical cylinder filled with a stationary liquid. The boundary conditions are $\mathbf{U}=0$ at walls. The bubble is initially at rest.

3. NUMERICAL METHOD

A control volume technique is used to discretise the PDEs. The computational domain is divided into a number of non-overlapping control volumes and all variables are defined at the centre of the control volume. Such a collocated arrangement of the grid may reduce the accuracy of the diffusive term, but it has advantages, such as an accurate representation of flux and source

terms. The collocated grid is illustrated in Figure 2. The differential equations are integrated over each control volume. For any variable, ϕ, The time integral over a cell P is given by

$$\int_{\Delta\Psi}\left(\frac{\partial\phi}{\partial\tau}\right)d\Psi=\frac{\phi_{i,j,k}^{n+1}-\phi_{i,j,k}^{n}}{\Delta\tau}\Delta\Psi \qquad (12)$$

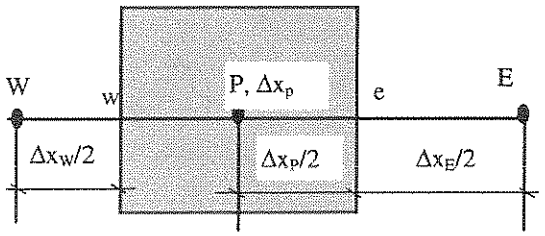

Figure 2: Schematic arrangement of a grid system in the x-direction

For the orthogonal grid used in this study, convection and diffusion terms are written after integration as

$$\int_{\Delta\Psi}\left[\nabla\cdot(G\phi)-\nabla\cdot(\Gamma\nabla\phi)\right]d\Psi=(J^{D}+J^{C})_{e}-(J^{D}+J^{C})_{w}+(J^{D}+J^{C})_{n}-(J^{D}+J^{C})_{s}+(J^{D}+J^{C})_{t}-(J^{D}+J^{C})_{b} \qquad (13)$$

For example, the diffusion contribution at the east face of the control volume P, J_e^D, is linearised by central differencing as

$$J_{e}^{D}=-\left(\Gamma\frac{\partial\Phi}{\partial x}A\right)_{e}=-\frac{\left[\alpha_{2e}\Gamma_{E}+(1-\alpha_{2e})\Gamma_{P}\right]}{0.5(\Delta x_{P}+\Delta x_{E})}(\Phi_{E}-\Phi_{P})A_{e} \qquad (14)$$

The linearisation of the diffusion terms on other faces are similar. It should be noted that the accuracy of a solution may be reduced if $\Delta x_P \neq \Delta x_E$ in equation (14). The convection contribution is given by a generalised form with the well-known deferred correction expression as,

$$J_{e}^{C}=G_{e}^{+}\Phi_{P}+G_{e}^{-}\Phi_{E}+(G\Phi)_{e}^{dc} \qquad (15)$$

in which, the first-order upwind mass flux is defined by

$$G_{e}^{+}=\frac{G_{e}+|G_{e}|}{2},\qquad G_{e}^{-}=\frac{G_{e}-|G_{e}|}{2} \qquad (16)$$

and

$$(G\phi)_{e}^{dc}=\left[\alpha_{1e}\phi_{E}+(\alpha_{2e}-1)\phi_{P}-q_{e}(\phi_{E}-\beta_{2e}\phi_{P}+\beta_{1e}\phi_{W})\right]G_{e}^{+}+\left[(\alpha_{2e}-1)\phi_{E}+\alpha_{1e}\phi_{P}-q_{e}(\phi_{P}-\beta_{2e}\phi_{E}+\beta_{1e}\phi_{EE})\right]G_{e}^{-} \qquad (17)$$

For a uniform grid, the geometric parameters are equal to $\alpha_{1e}=0.5$, $\alpha_{2e}=0.5$, $\beta_{1e}=1$ and $\beta_{2e}=2$ respectively. By varying the deferred correction term, a higher order scheme for the convection term can be obtained (see Li [1997] for details). For a uniform grid, in the second-order central differencing (CD), $q_e=0$; q_e is equal to 1/8 or 1/6 for a second- or third-order accurate QUICK scheme respectively, and equal to $\max\{0,0.5-1/|Pe_e|\}$ for the second-order HYBRID scheme (SHYBRID). The flux G_e is calculated by Rhie-Chow's interpolation technique. This technique effectively overcomes the difficulty of the decoupling between pressure and velocity raised from a linear interpolation and guarantees a global mass conservation.

As the grid point is always located at the center of a control volume, a representative source is obtained by

$$\int_{\Delta\Psi}sd\Psi=s_{P}\Delta\Psi_{P} \qquad (19)$$

The surface tension force is linearised by a 27-point stencil for a three-dimensional surface. The detail of an implementation can be found in Chen et al. [1996].

To capture the sophisticated dynamics of an interface, an accurate technique is needed to solve equation (11). In this study, a modified line constant VOF method is used (see Chen et al. [1997]). In this method, the interface tracking is divided into three steps: (1) reconstruct the surface based on the calculated unit normal to the surface, which is required in the surface tension calculation; (2) advect the surface with local velocity using the first-order upwind or downwind schemes; (3) bookkeeping to guarantee the value of each local volume fraction F does not to exceed the range of 0 to 1. The upwind scheme is numerically diffusive; and a downwind scheme has the advantage of maintaining the sharpness of a surface, but it is numerically unstable. In the original VOF method, a surface can only be considered as either parallel or horizontal to the flux direction, thus the numerical diffusion is unavoidable in some flow situations, such as when a surface has an 45° angle to the velocity field. In our modified VOF, the upwind and downwind schemes are combined based on the surface orientation to achieve an accurate advection of a surface. When a surface is considered as parallel to the flux direction, the upwind scheme is used, otherwise the downwind scheme is used. The definition of parallel or perpendicular to the flux direction is determined by the resective component of the unit normal to a surface, $\hat{\mathbf{n}}(n_r,n_\theta,n_z)$, in equation (9). It can be adjusted based on the velocity field. Due to the constant line structure of a surface adopted, special care is required to restrict an over- or under-flux when the downwind scheme is used. The implementation details can be found in Lafaurie et al. [1994]. It is believed that a slope-line VOF method, e.g. Youngs' method [1982], overcomes such a over- or under-flux problem and is able to produce a better result. Youngs' method has not been implemented here.

To demonstrate our front tracking method, a test problem of a spherical bubble axisymmetrically rising in

a liquid with a constant velocity field $U(u_r, u_z) = (0,0.5)$, has been performed. It can be seen from Figure 3b that when a pure upwind scheme is used, i.e. n_r or $n_z = 1$ for r or z components of equation (11) respectively, a serious smear of the sphere is observed after 500 iterations due to the numerical diffusion. Switching to the downwind scheme whenever the angle between a surface and flux direction is greater than 21.8° (n_r or $n_z \geq 0.4$), the numerical diffusion is greatly reduced and only a slightly smeared surface at the first quarter of the sphere is observed (see Figure 3c). However, a pure downwind scheme, n_r or $n_z = 0$, results in flotsam, as may be seen in Figure 3d.

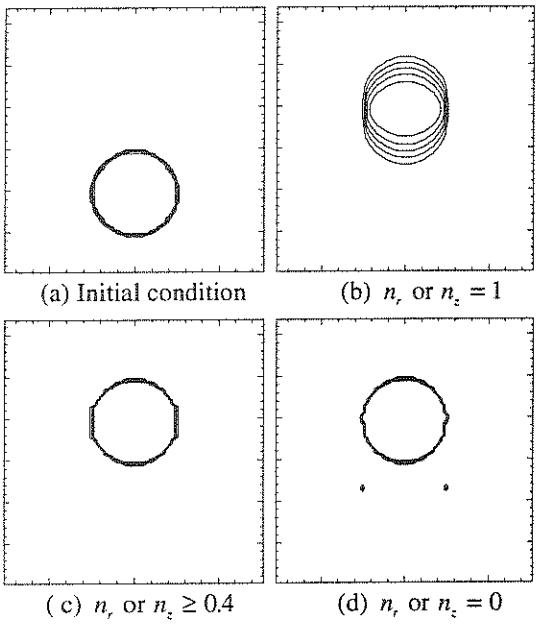

Figure 3: Translation of a sphere with different combination of the upwind and downwind schemes ($\Delta z = \Delta r = 0.04$, $\Delta t = 0.01$, at 500th iteration)

A semi-implicit scheme is used to solve equation (2) for the velocity field and the SIMPLE method is adopted for the velocity-pressure coupling. The resultant non-symmetrical system arising from the momentum equation is solved by the SIP or Bi-Conjugate Gradient method with the Incomplete Cholesky preconditioning. The symmetric system due to pressure correction is solved by the Conjugate Gradient method with the Incomplete Cholesky preconditioning.

4. RESULTS AND DISCUSSION

A grid-independent test was carried out on the axisymmetric rise of a single bubble in a liquid. The bottom position of the bubble as a function of time is illustrated in Figure 4 with three different meshes (N_z by N_r): 54 by 17, 108 by 34 and 216 by 68, which corresponds to 145, 578 and 2312 grid points in the rectangle containing the hemisphere region. It can be seen that meshes 108 by 34 seem to produce a near grid-independent solution. This grid size will be used in all other runs.

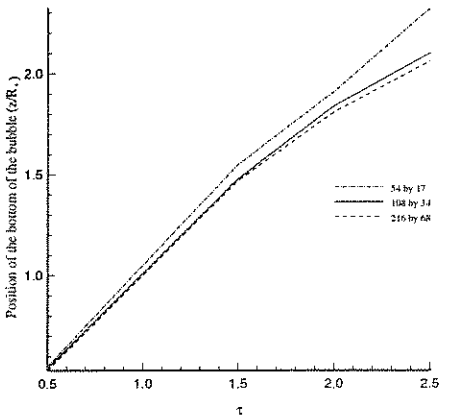

Figure 4: Effect of grid size on the position of a bubble risine in an cylinder ($Bo = 50$, Re = 100, $\rho_f/\rho_g = 80$, $\mu_f/\mu_g = 80$)

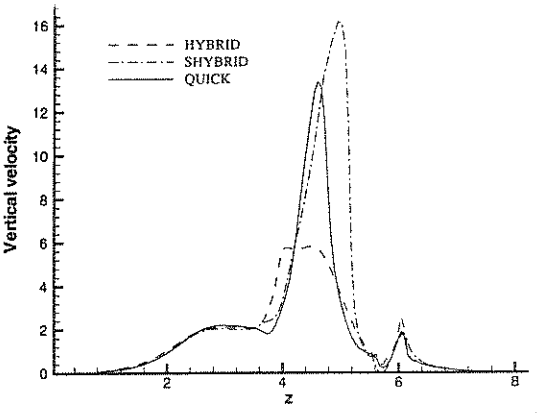

Figure 5: Vertical velocity profile along z-axis with different convection schemes

In order to validate the predicted results with available experimental data, the axisymmetric rise of two gas bubbles of the same size in a very viscous liquid with a high density ratio is simulated. The parameters used in the simulation are chosen to be close to the experimental conditions and are Re = 10, $Bo = 50$, $\rho_f/\rho_g = 850$ and $\mu_f/\mu_g = 100$. The non-dimensional initial distance between two bubbles is 0.36.

Generally, when a single bubble rises due to the buoyancy force, the pressure gradient at the lower surface of the bubble is higher than the one at the top surface of the bubble, and the vortex sheet which develops at the surface has a sense of rotation which induces a tongue of liquid jet that pushes into the bubble from below. Deformations of the bubble occur. This phenomenon was reported by many experimentalists, e.g. Walters and Davidson [1963]. For multi-bubble rising, similar behaviour is expected but the deformation and fragmentation of surfaces are more complex. Therefore the use of a higher-order convection scheme

is necessary to catch the liquid jet accurately. The effect of the convection scheme was studied. As may be expected, for bubble rise with a low Reynolds number, $\mathrm{Re}=10$, the SHYBRID scheme produces the same results as the HYBRID because most of the grid Peclet numbers are less than 2 and, effectively, the central differencing is used in both schemes. However, with a higher Reynolds number $\mathrm{Re}=100$, the differences between different schemes are clear, as may be seen in Figure 5. The HYBRID scheme under-predicts the jet and a smeared solution of the velocity field is obtained. The SHYBRID over-predicts the jet. The third-order QUICK scheme seems to well predict the resolution of the liquid jet in terms of both its maximum value and location. Therefore QUICK is used in the following studies.

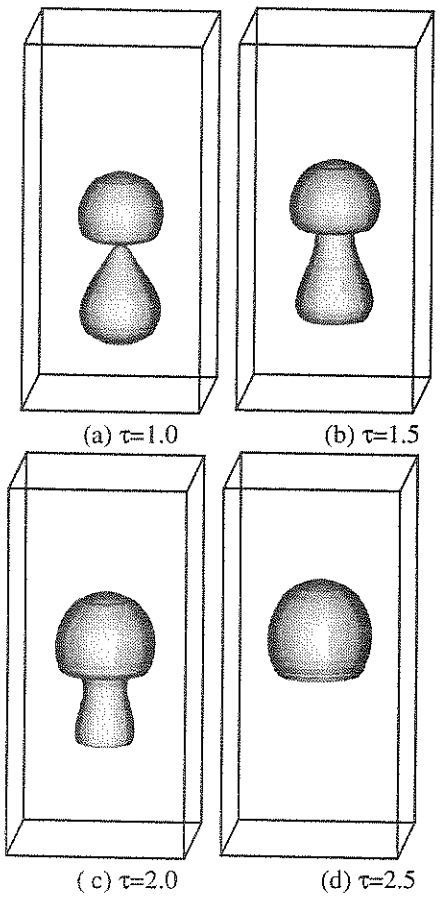

Figure 6: Predicted the axisymmetric coalescence of two gas bubbles in a very viscous liquid (Re=10, Bo=50, ρ_f/ρ_g=850, μ_f/μ_g=100, z/R_0=0.36)

For two-bubble coalescence in highly viscous glycerin liquid, a preliminary comparison between the predicted results and the experimental observations (Figure 2 in Narayanan et al. [1974]) was performed. The similarity of the shape development of two bubbles in the highly viscous liquid can be clearly seen from Figures 6 and 7. Because of a lack of details of the experiment, no quantitative comparison is possible.

It can be seen from Figure 6 that the motion of the leading bubble induces a deformation in the following bubble, giving it a pear-like shape (Figures 6a,b). Once two bubbles are approaching (Figure 6b), an acceleration of the following bubble is obtained due to a low pressure region behind the leading bubble, which is evidenced by the non-linear behaviour of the top position history of the following bubble in Figure 8. As time progresses, the two bubbles start to touch, as may be seen in Figure 6c, leaving a mushroom-like structure. The two bubbles travel as a single bubble, then a further fragmentation occurs and a larger spherical cap is obtained, as may be seen in Figure 6d. A detailed study of the motion of such a single bubble in a viscous liquid, such as the formation of a toroidal bubble, can be found in Chen et al. [1996].

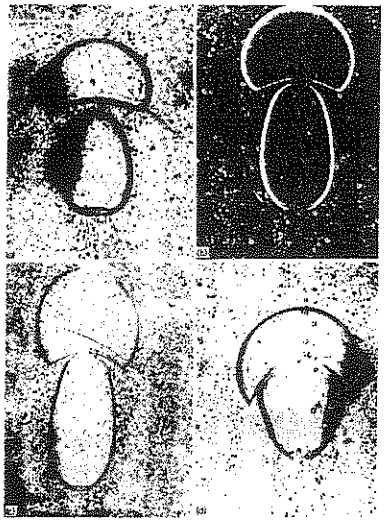

Figure 7: Experimental result of the coalescence of two air bubbles in glycerin liquid by Narayanan [1974]

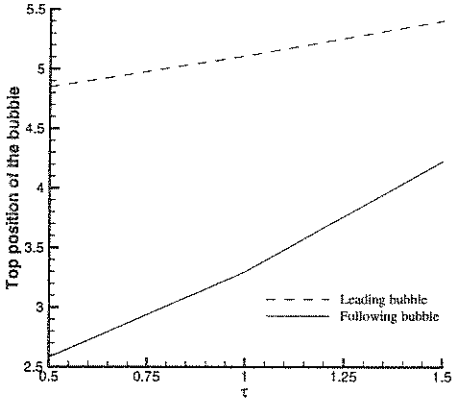

Figure 8: Top positions of leading and following bubbles as a function of time

The details of the coalescence of the two bubbles are shown in Figure 9 for velocity field and three contour lines of function F: 0.1, 0.5 and 0.9. It can be seen that the liquid circulation around the bubble produces a jet to push the lower surface of both leading and following

bubbles and the deformations of the bubbles occur (Figure 9a). Due to the effect of the velocity field around the leading bubble, the following bubble is stretched and a spherical cap-shaped leading bubble is observed (Figure 9b), which are similar to the experimental results in Figure 8. After the coalescence occurs, the lower surface of the merged bubble is accelerated by the liquid jet and a larger spherical cap is obtained (Figures 9c,d). The contour lines of F in Figure 9 have shown an accurate representation of the bubbles with minimum numerical diffusion.

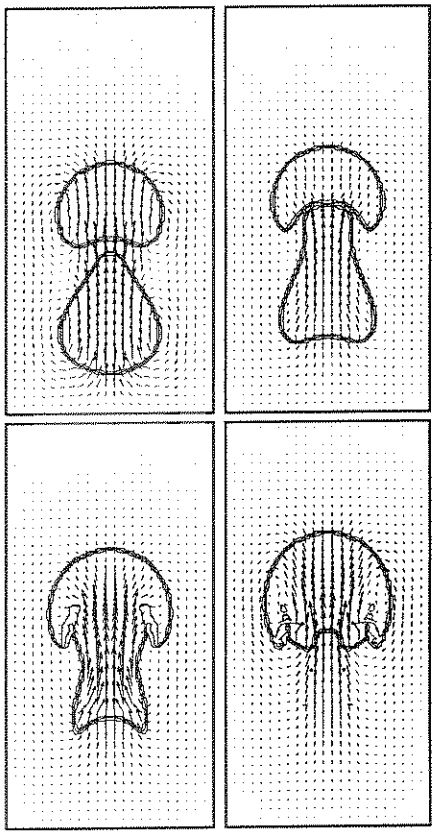

Figure 9: Velocity field and three contours of F of the values of 0.1, 0.5 and 0.9 for the simulation in Figure 6

5. CONCLUSION

A robust numerical model for a two-phase fluid system with a high density ratio has been presented. The model accounts for surface tension and adopts high-order convection schemes and a semi-implicit technique. The modified VOF method has shown to have the capability to capture a complex surface with a reasonable accuracy and its implementation for three-dimensional flows is straightforward. The coalescence of two gas bubbles in a highly viscous liquid has been simulated. It has been found that complex deformation and fragmentation of interfaces can be well predicted by the present model and a reasonable agreement between numerical simulation and experimental results has been achieved.

6. ACKNOWLEDGEMENTS

The original development of the code used in this study was carried out in UNSW under the supervision of Professors J. A. Reizes and E. Leonardi.

7. REFERENCES

Brackbill, J.U., D.B. Kothe, and C. Zemach, A continuum method for modeling surface tension, *J. Comp. Phys.*, 100, 335-354, 1992.

Chen, L., S.V. Garimella, J. A. Reizes, and E. Leonardi, Analysis of bubble rise using the VOF Method: I isolated bubbles, *ASME Proceedings of the 31st NHT Conference*, Houston, 4, 161-173, 1996

Chen, L., S.V. Garimella, J.A. Reizes, and E. Leonardi, Motion of interacting gas bubbles in a viscous liquid including wall effects and evaporation, *Num. Heat Transf., Part A*, 31, 629-654, 1997.

Hirt, C. W. and B.D. Nichols, Volume of fluid (VOF) method for the dynamics of free boundaries, *J. Comp. Phys.*, 39, 201-225, 1982.

Lafaurie, B., C. Nardone, R. Scardovelli, S. Zaleski, and G. Zanetti, Modelling merging and fragmentation in multiphase flows with SURFER, *J. Comp. Phys.*, 113, 134-147, 1994.

Li, Y., Wavenumber-extended high-order upwind-biased finite-difference schemes for convective scalar transport, *J. Comp. Phys.*, 132, 235-255, 1997.

Narayanan, S., H.J. Goossens, and N.W.F. Kossen, Coalescence of two bubbles rising in line at low Reynolds Numbers, *Chem. Eng. Sci.*, 29, 2071-2082, 1974.

Rider, W.J., D.B. Kothe, J. Mosso, and J.H. Cerutti, Accurate solution algorithms for incompressible multiphase flows, *AIAA*-95-0699, 1-17, 1995.

Ryskin, G. and L.G. Leal, Numerical solution of free-boundary problems in fluid mechanics - Part 2, buoyancy-driven motion of a gas bubble through a quiescent liquid, *J. Fluid Mech.*, 148, 19-35, 1984.

Unverdi, S.O. and G.A. Tryggvason, front-tracking method for viscous, incompressible, multi-fluid flows, *J. Comp. Phys.* 100, 25-37, 1992.

Walters, J. K. and J.F. Davidson, The initial motion of a gas bubble formed in an inviscid liquid - Part 2. the three-dimensional bubble and the toroidal bubble, *J. Fluid Mech.*, 17, 321-336, 1963.

Youngs, D. L., Time-dependent multi-material flow with large fluid distortion, *Numerical Methods for Fluid Dynamics*, K. W. Morton and M.J. Baines Editors, 273, 1982.